to be presented at the American Controls Conference, June 6, 1997

Integrated Modeling Methodology Validation Using the Micro-Precision Interferometer Testbed: Assessment of Closed-Loop Performance Prediction Capability

James W. Melody
jmelody@csi.jpl.nasa.gov
(818) 354–0615

Gregory W. Neat
neat@huey.jpl.nasa.gov
(818) 354–0584

Jet Propulsion Laboratory,
California Institute of Technology
4800 Oak Grove Drive
Pasadena, CA 91109

Abstract

This paper validates the integrated modeling methodology used for design and performance evaluation of complex opto-mechanical systems, particularly spaceborne interferometers. The methodology integrates structural modeling, optical modeling, and control system modeling and design into a common environment, the Integrated Modeling of Optical Systems (IMOS) software package. The validation uses the Micro-Precision Interferometer (MPI) testbed, a ground-based, full-scale hardware model of a spaceborne interferometer. Parallel development of the MPI testbed and an MPI integrated model enabled a unique opportunity to validate the modeling methodology with actual testbed measurements. This paper assesses the ability of the integrated modeling methodology to predict performance in a closed-loop configuration, namely with high-bandwidth optical control loops operational. The assessment is a comparison of integrated model closed-loop predictions with MPI testbed closed-loop measurements, indicating that the integrated modeling methodology is accurate to within a factor of three.

1 Introduction

Discovery of earth-like planets around other stars requires an instrument with micro-arcsecond astrometric measurement accuracy [1, 2]. Spaceborne optical interferometers are likely to be the first instrument class capable of achieving this accuracy level. Although this partial-aperture approach offers a number of important advantages over the traditional full-aperture

approach (*e.g.*, the Hubble Space Telescope) the instrument requires stabilization of optical elements down to the nanometer level as well as laser metrology resolution at the picometer level [3]. The charter for the JPL Interferometer Technology Program (ITP) is to mitigate risk for this optical interferometer mission class [4]. A number of ongoing complementary activities address these technology challenges. These activities are: integrated modeling methodology development and validation, metrology and vibration hardware testbed development, and flight qualification of the interferometer components. Though all of these activities are necessary to buy down mission risk, it is integrated modeling that ultimately will be used in the mission and instrument design. This paper investigates the ability of the integrated modeling methodology to meet these demanding analysis needs.

In anticipation of these needs, the Integrated Modeling of Optical Systems (IMOS) and the Controlled Optics Modeling Package (COMP) software packages were developed at JPL [5, 6]. The integrated modeling methodology combines structural modeling, optical modeling, and control system design and modeling within a common software environment. Coincident with this development, the Micro-Precision Interferometer (MPI) testbed was built to assess vibration attenuation technologies on a dynamically and dimensionally representative hardware model of a spaceborne interferometer (see Figure 1) [1].

An integrated model of MPI was developed in parallel with the testbed. This modeling/hardware synergy resulted in a unique opportunity to validate the modeling methodology by comparing model predictions with testbed measurements. Disturbance transfer functions, measured from the attachment point of the primary disturbance source (spacecraft reaction wheel assemblies) to output optical sensors, are the primary measurements used for model validation. These transfer functions accurately depict (in a linear sense) the effectiveness of vibration attenuation strategies at achieving nanometer stabilization of optical elements on a large, lightly-damped, flexible structure excited by mechanical vibrations. The two most effective strategies are: 1) vibration isolation of the disturbance source to attenuate high-frequency disturbances and 2) high-bandwidth optical control to reject low-frequency and middle-frequency disturbances.

Exhaustive model validation requires model and testbed comparisons for three vibration attenuation configurations: 1) a hard-mounted disturbance source with an open-loop optical system, 2) a hard-mounted disturbance source with a closed-loop optical system and 3) an isolated disturbance source with a closed-loop optical system. Validation for the first configuration has been performed previously on the MPI testbed [7]. This paper addresses model validation for the hard-mounted, closed-loop configuration by presenting the closed-loop performance validation procedure, the optical control design, the closed-loop MPI integrated model, and the validation results.

2 Closed-Loop Validation Procedure

Figure 2 presents the integrated modeling methodology validation procedure for the closed-loop optics configuration. The figure depicts each step as either a hardware or an analysis procedure. In the first step, the open-loop, analytical model of the MPI structure and optics

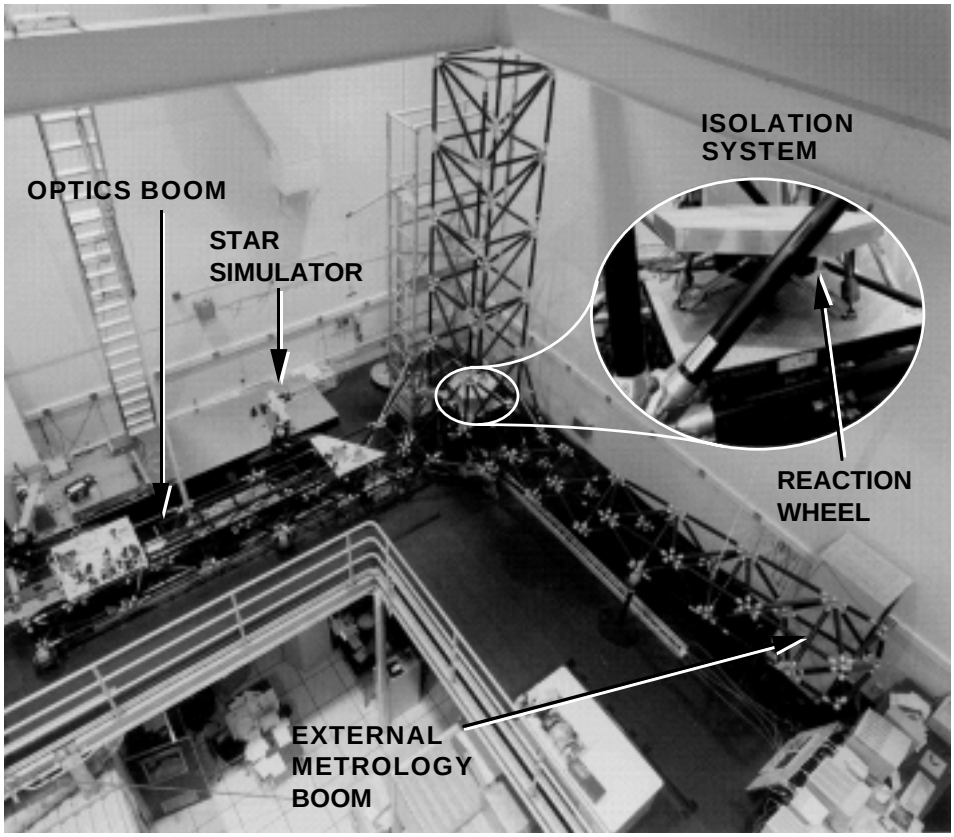

Figure 1: Bird's-eye view of the MPI Testbed.

is built with *a priori* knowledge of the structural geometry, material properties, and optical layout. The second and third steps are used to update the analytical model properties. Since the focus of this effort is to validate the integrated modeling *methodology*, a structural model with accurate properties is necessary so that deficiencies of the methodology can be investigated separately from inaccuracies of the model. Specifically, the material properties as well as the structural geometry itself have been refined (step three) based on modal test data acquired from the testbed (step two). These first three steps have been presented extensively in the literature [7, 8, 9].

As with the structural properties, validation of the modeling methodology necessitates the use of identical optical control system compensators in order to remove the effects of model inaccuracies. Identical compensators and the requirement of control stability place an implied requirement on the accuracy of the plant transfer functions (*i.e.*, from control input to measured output), particularly near the control bandwidths. The fifth step of Figure 2 uses the measured plant transfer functions from step four to adjust structural model parameters in order to improve the accuracy of the plant transfer functions. In step six an optical control system is designed for the testbed based on measured plant transfer functions. Design considerations include practical implementation issues such as the effect

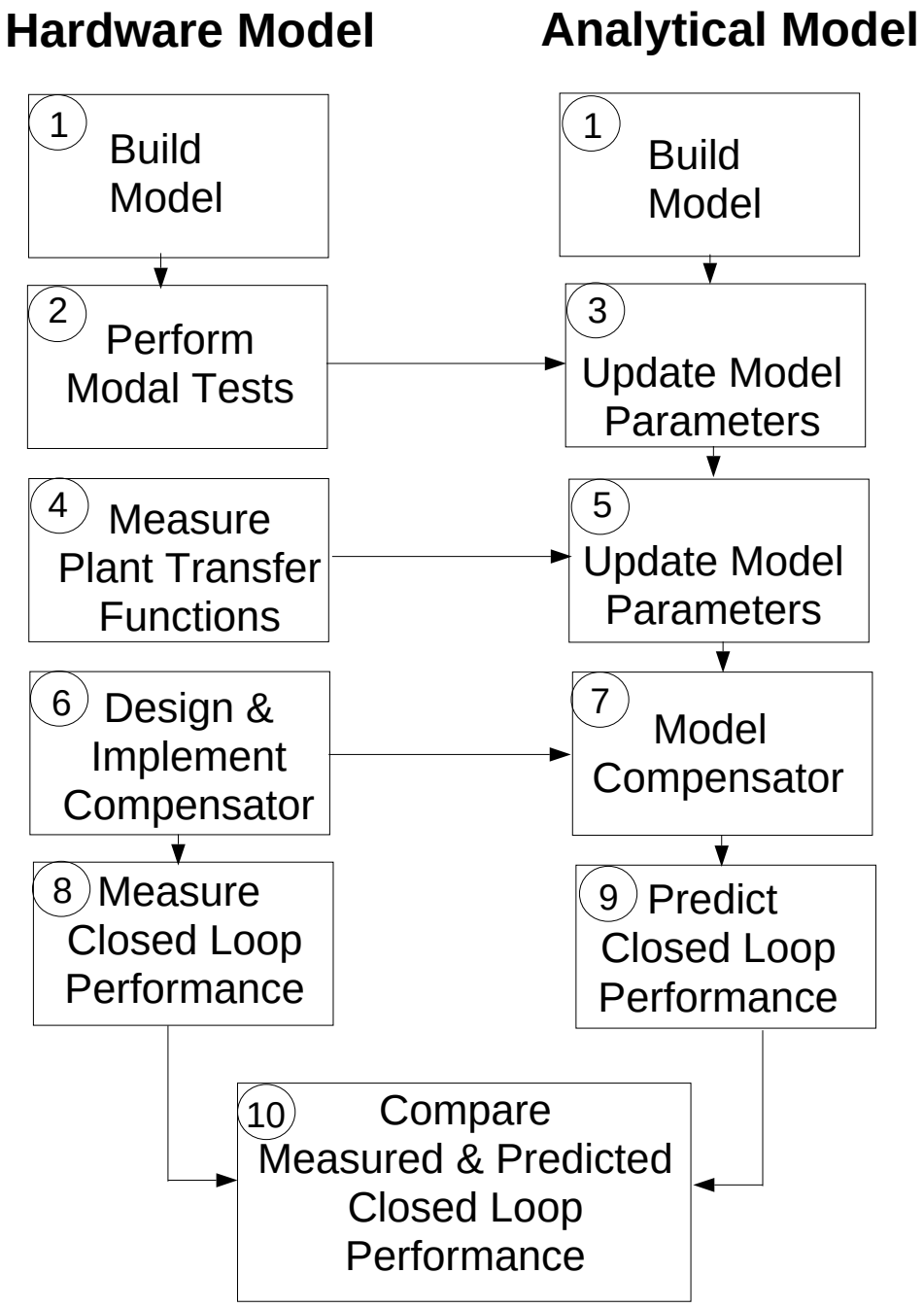

Figure 2: Closed-loop integrated modeling methodology validation procedure.

of sampling delays, quantization errors, actuator and sensor dynamic range limitations, and reasonable filter order. This compensator is modeled analytically and added to the integrated model in step seven. Disturbance transfer functions are measured in the laboratory (step eight) and predicted using the closed-loop integrated model (step nine). Finally in step ten, the resultant transfer functions are compared using the metric defined in [7].

3 Optical Pathlength Control System

The interferometer requires a number of optical control systems in order to perform a measurement. These consist of coarse starlight acquisition, fine pointing, and pathlength control. While acquisition and pointing control enable measurement of the interference fringe, it is the pathlength control system that directly controls the optical quantity of scientific interest, stellar pathlength. In particular, the purpose of the pathlength control system is to equalize stellar pathlength from the observed star through each arm of the interferometer to the detector. The pathlength control system must stabilize this optical path difference (OPD) down to 10 nm (RMS) in the presence of the reaction wheel disturbances. Figure 3 shows a complete block diagram of this control system.

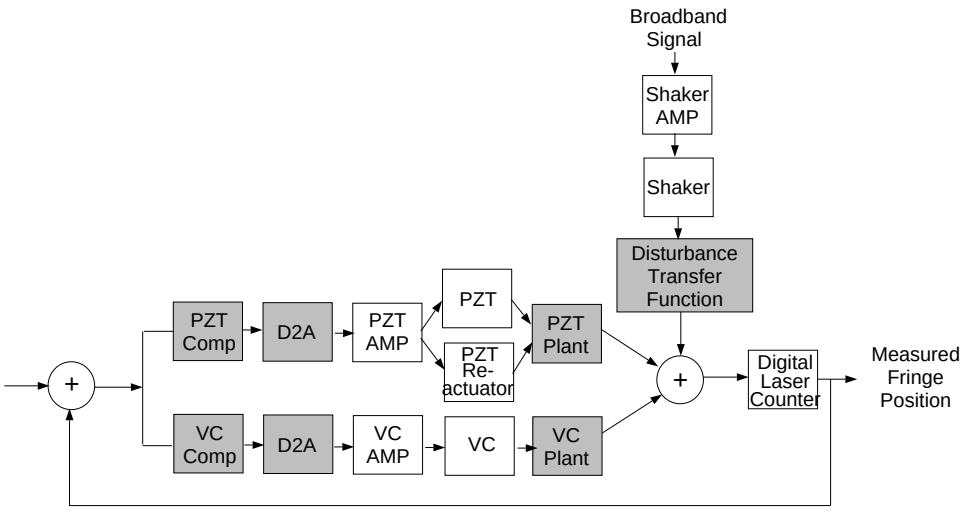

Figure 3: Block diagram of the pathlength control system.

The pathlength control system actuator has three stages and acts as a linearly translating optical delay line with tremendous dynamic range. The three stages are: a stepper motor for low-frequency (dc), long-travel capability (1 m); an intermediate voice-coil actuator for medium-frequency (dc – 100 Hz), medium-amplitude control (cm); and a reactuated piezo-electric device (PZT) for high-bandwidth (up to kHz), precise actuation (μm). Whereas the stepper motor enables stellar acquisition, the PZT and voice coil provide the actuation necessary to reject disturbances during an interferometer stellar measurement. Hence only the voice coil (VC) and piezo-electric device (PZT and PZT reactuator) are shown in Figure 3.

The sensor for this system is a mono-chromatic fringe detector, shown as the digital laser counter in Figure 3. This optical sensor measures the amplitude and phase of the stellar OPD at the nanometer-level.

The control system requirements dictated by interferometer performance are: 1) open-loop 0 dB crossover frequency at or below 400 Hz, 2) gain margins of 6 dB and phase margins of 30^o, 3) maximum disturbance rejection over the allowed bandwidth, and 4) conditional stability is acceptable. The control system requirements dictated by the implementation procedure for this validation are: 1) digital sample rate of 8 kHz, 2) all compensator poles and zeros must be above 0.1 Hz, and 3) the total number of compensator states must be less than 10.

The shaded boxes in Figure 3 represent the elements explicitly modeled in this validation process. Actuators and amplifiers are assumed to have no dynamics or range limitations, and sensors are assumed to be noise free. Hence they are not explicitly modeled.

4 MPI Integrated Model

The MPI integrated model consists of a structural finite element model, a linear optical model, and a controls model integrated together. The structural and optical models are described in detail in [7] and are summarized below. The high-bandwidth optical control system model and design are described in greater detail below. The structural model is generated with IMOS, whereas both IMOS and COMP are used to create the optical model. The integration, control system modeling, and disturbance analysis are performed in MATLAB with the aid of IMOS functions.

4.1 Structural Model

The structural model is specified in IMOS as a finite element geometry, shown in Figure 4. This geometry consists of plate, beam, truss, and rigid body elements modeling the base truss structure and the attached components (for precise definition of these elements, see [5]). A modal damping of 0.3% is assumed for the global flexible-body modes, and a damping of $\approx$3% is assumed for the dynamics associated with the delay line structure. These damping values are consistent with estimates obtained from modal tests. Overall, the finite element model uses 2,577 degrees of freedom (dof) of which 1,832 dofs are independent with respect to the multi-point constraints of the rigid body elements (RBEs) [5, 7].

4.2 Optical Model

The optical model begins with a specification of the optical prescription. This prescription includes the shapes, positions, and orientations of the optical elements. A ray trace of the optical prescription is shown in Figure 5. Note that Figure 5 highlights the location of the pathlength control system actuator and sensor. This optical prescription is generated in IMOS based on the prescription of the actual optical elements of MPI.

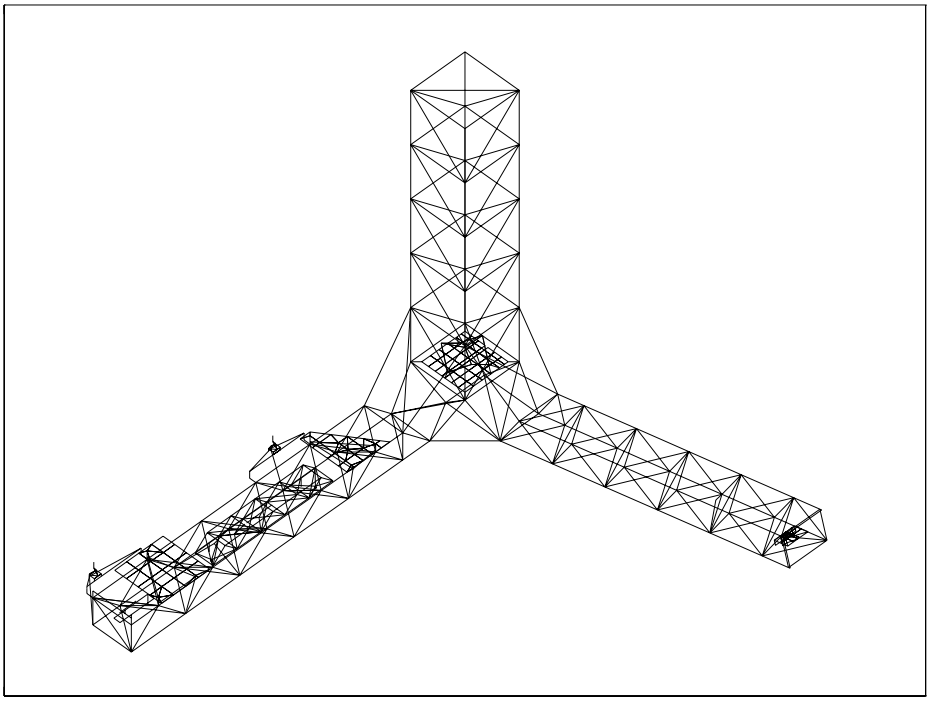

Figure 4: MPI finite element geometry (compare with Figure 1).

Once the optical prescription is specified, it is exported to COMP where a linear optical model is created. This linear model is calculated by performing an analytic differential ray trace [6]. The optical output can be pathlength, wavefront tilt, or spot motion. For this validation study the output is pathlength difference.

4.3 Structural-Optical Model Integration

Once the structural and optical models have been created, they are integrated to form a structural-optical model. This integrated model is specified in first-order, state-space form, lending itself most easily to analysis and control synthesis with existing MATLAB functions.

First, the structural model is truncated to remove modes above the bandwidth of expected disturbances (*i.e.*, above 900 Hz) [10]. The truncated modal model is then converted into first-order, state-space form [5, 7]. Finally, the linear optical model is incorporated. The resulting model has disturbance forces, delay line PZT command (including reactuation), and delay line voice-coil command as input. The output is stellar OPD.

4.4 Control System Model and Design

Given the integrated structural-optical model in first-order, state-space form, optical control synthesis and modeling are performed with MATLAB Control System Toolbox functions.

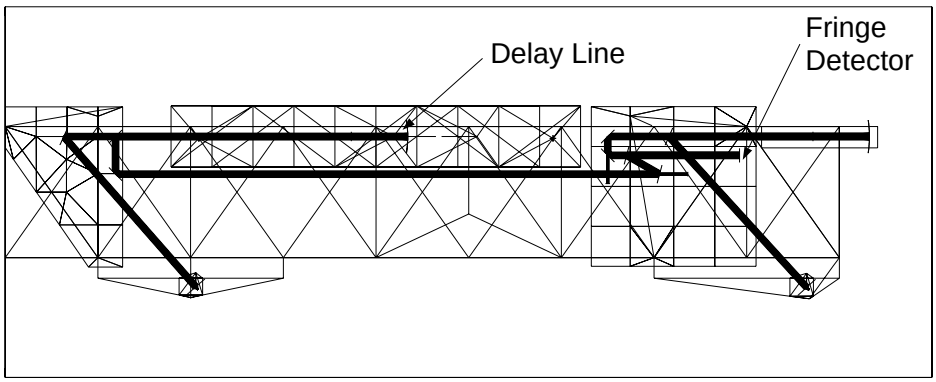

Figure 5: Ray trace of the MPI optical prescription on the finite element geometry of the optics boom.

The resulting model is also in state-space form, with disturbances as input and stellar OPD as output.

The control system model was based on the compensator designed for the testbed. The phase loss inherent to a digital control system was modeled as a pure time delay of 0.3 ms. The remainder of the control system model was a continuous-time representation of the following design.

The basic design strategy is to use the two actuators in a parallel configuration, facilitating the separation of actuator dominance into specific frequency bands. This design approach requires that attention be paid not only to the open-loop 0 dB crossover, but also to the relation between the parallel paths, particularly near the frequency where the two actuator loop-gains are equal in magnitude (the actuator "hand-off" frequency). The actuator dynamic ranges and the anticipated disturbance spectrum are considered in determining this hand-off frequency. For this design, the hand-off frequency is 7 Hz. The design must also ensure that a single actuator dominates in the respective frequency bands. In other words, there must be a sufficient loop-gain separation between the voice coil and the PZT both above and below the hand-off frequency.

Figure 6 shows the predicted loop gains of the PZT, the voice coil, and the parallel combination (*i.e.*, the total loop gain for the system). Stability assessment with this approach requires two functions to be Nyquist stable: 1) the total loop gain and 2) the function defined by the ratio of the voice-coil loop gain and the PZT loop gain [11]. References [12, 13] provide more details on this control system design.

5 MPI Testbed

The testbed compensator was designed based on measured voice-coil and PZT plant transfer functions. The compensator represented in Figure 6 was implemented in C on the VME-based realtime computer system of the testbed [1]. The control system utilizes a single 68040

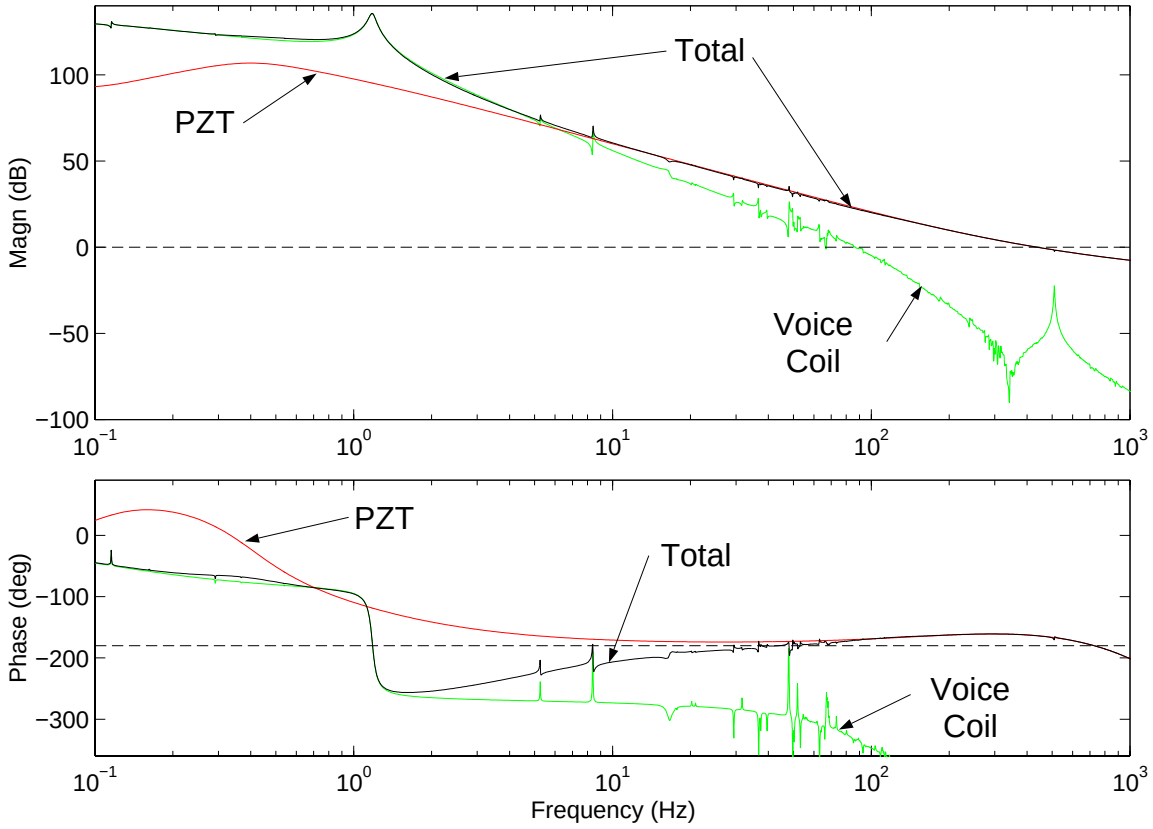

Figure 6: Optical delay line loop gains.

processor that provides the voice-coil and PZT command signals at an 8 kHz rate.

The disturbance transfer functions were measured for three force disturbance directions: (x, y, z). An HP data analyzer was used to collect the data. A 10 N shaker, mounted at the base of the tower, applied the force input in each of the three directions. The force input was derived from an accelerometer mounted to the shaker proof mass. The analyzer calculated the transfer functions from force input to OPD output.

6 Results

The metric used to compare the measured and predicted transfer functions for the open-loop validation [7] will be used for the closed-loop comparision. This metric, σ_g, is based on the the variance of resulting OPD when the disturbance is band-limited white noise:

$$\sigma_g^2 = \frac{A_d}{\pi} \int_{f_{min}}^{f_{max}} |G(j\omega)|^2 d\omega \tag{1}$$

where A_d is the amplitude of the bandlimited white noise disturbance power spectral density with f_{min} and f_{max} defining the frequency range of interest.

Using this metric, the accuracy of the model can be quantified by comparing σ_g for the predicted and measured transfer functions. As such, the particular value of the disturbance amplitude is immaterial, hence A_d is chosen arbitrarily. Generally, it is desired that OPD variation predictions be accurate to within a factor of 2. Since the metric σ_g is closely related to OPD variations for broadband noise, the factor of 2 is applied as a requirement to the ratio of σ_g for the measured and predicted transfer functions. This goal was met for the open-loop validation study [7].

The modulus of the measured transfer functions, along with the corresponding predicted transfer functions, are shown in Figures 7-9. The predicted transfer functions were calculated by applying standard MATLAB functions to the integrated model with disturbance force input and OPD output. The value of the broadband metric, also calculated with MATLAB functions, is given in the legend for each transfer function.

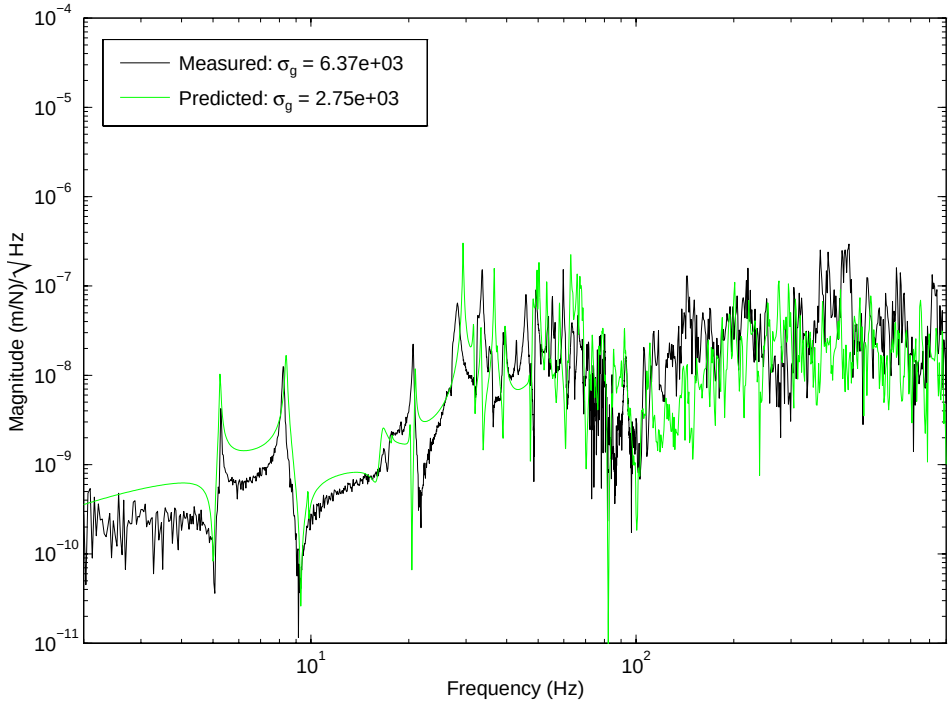

Figure 7: Predicted and measured MPI disturbance to OPD transfer function: x-axis force input.

The results of these comparisons are shown in Table 1. The "factor" entry is the ratio of σ_g for the measured and predicted transfer functions. The bandwidth of interest is [4, 900] Hz. Below 4 Hz the force capability of the shaker is limited and the testbed suspension modes pollute the measurement. Above 900 Hz the mechanical disturbances are expected to have no energy. This bandwidth is further broken roughly into decades and comparisons are shown for these "decades." Units are not given in the table so as to discourage the reader from attaching significance to the separate values.

In addition, Figure 10 compares the measured and predicted voice coil transfer functions.

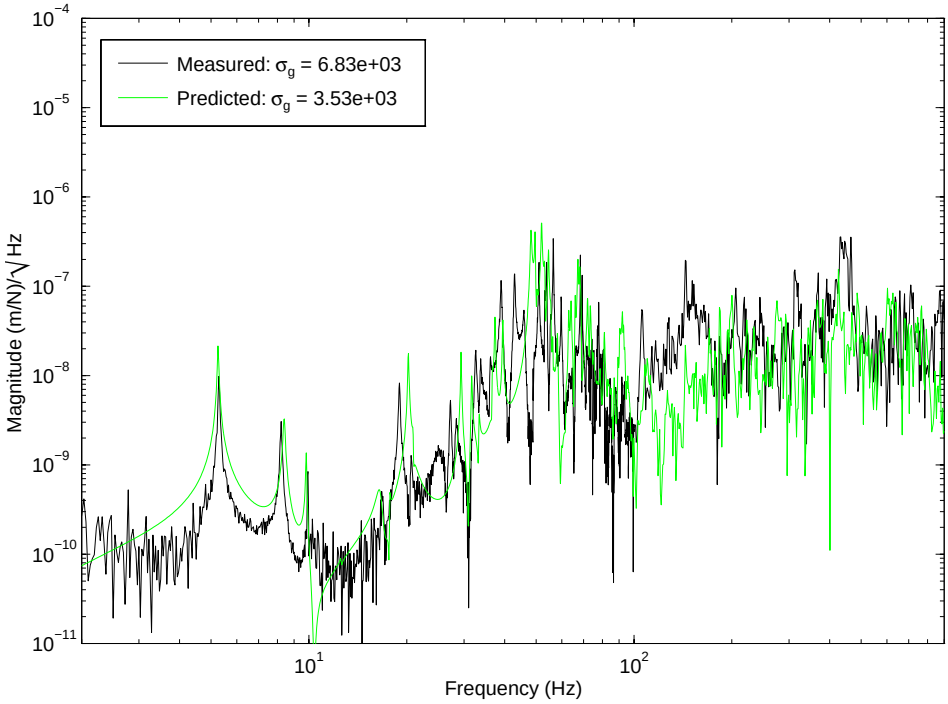

Figure 8: Predicted and measured MPI disturbance to OPD transfer function: y-axis force input.

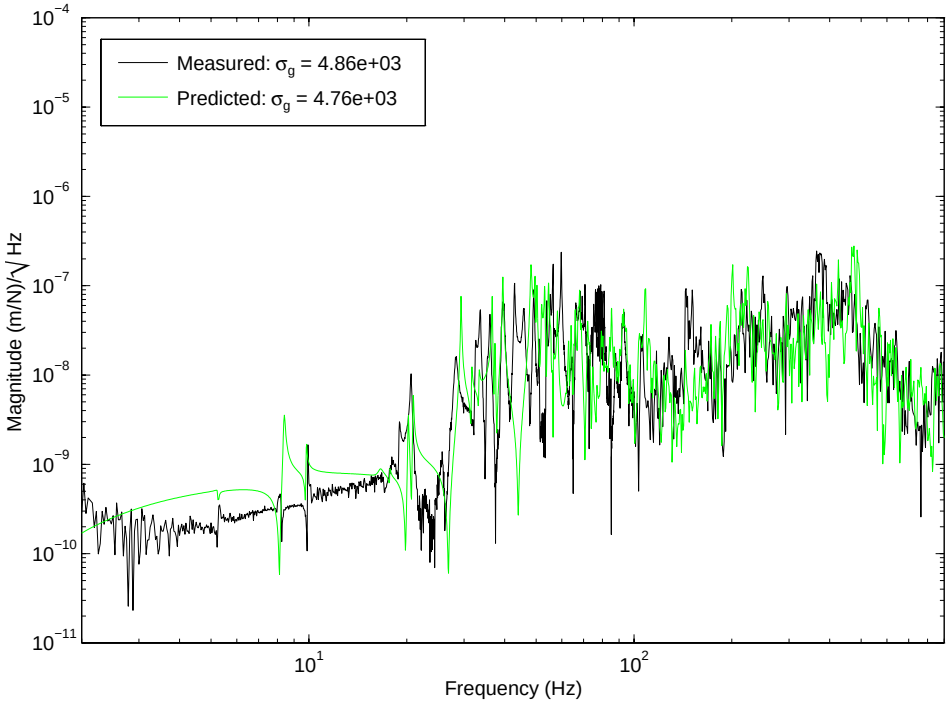

Figure 9: Predicted and measured MPI disturbance to OPD transfer function: z-axis force input.

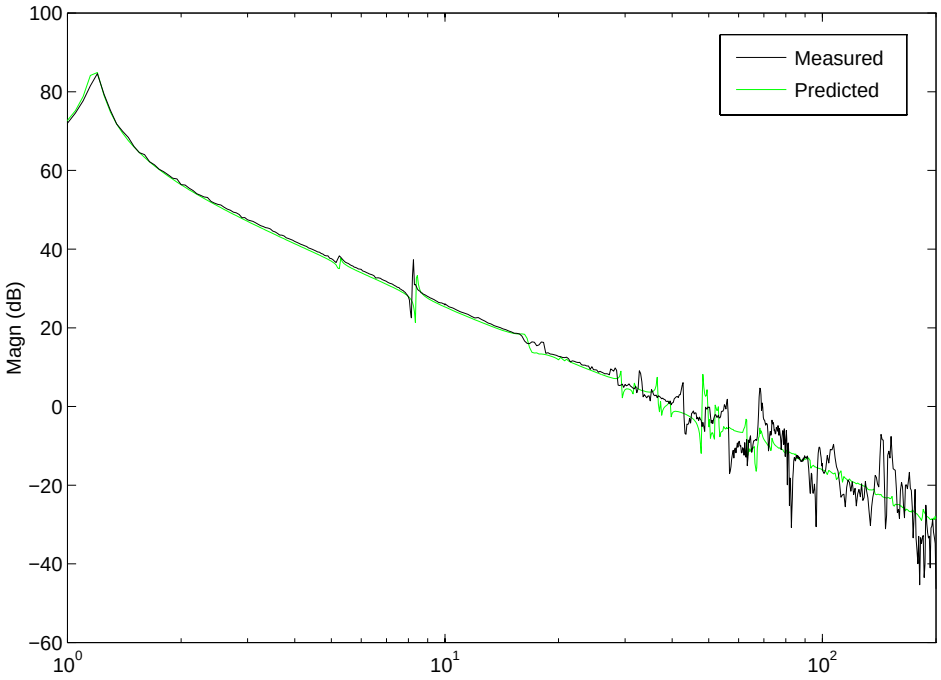

Figure 10: Predicted and measured MPI voice-coil plant transfer functions.

Of course, the integrated model was sufficiently accurate for the compensator designed on the testbed to result in a stable system when applied to the model.

The comparisons for the three force disturbance transfer functions show that the broadband metrics ([4, 900] Hz) for the predicted transfer functions are within a factor of three of the measurements. Note that this is not as accuarate as the open-loop validation, where a factor of two for the broadband metric was achieved [7]. One explanation for this is that the high-bandwidth optics significantly attenuate the low- and middle-frequency regions of the disturbance transfer function, leaving the majority of the energy in the high-frequency range. As is generally expected, the model is least accurate in this range. This was true even for the open-loop model, where comparisons for the high-frequency range ([100, 900] Hz) were accurate only to a factor of three. Another explanation is that the closed-loop system is more complex than the the open-loop case. In the open-loop study, only the "disturbance transfer function" box of Figure 3 is pertinent, whereas with this study, all of the boxes in Figure 3 pertain.

7 Conclusion and Future Work

This paper validates the performance prediction capabilities of the integrated modeling methodology which incorporates the IMOS and COMP analysis tools. This study addressed the hard-mounted disturbance, active-optics configuration. Results demonstrate model pre-

Disturbance Input		σ_g			
		4 - 10 Hz	10 - 100 Hz	100 - 900 Hz	*4 - 900 Hz*
x-axis Force	meas	16	723	6,329	*6,370*
	pred	26	1,167	2,485	*2,746*
	factor	1.59	1.61	0.39	*0.43*
y-axis Force	meas	9	1,025	6,750	*6,827*
	pred	20	2,158	2,799	*3,535*
	factor	2.16	2.11	0.41	*0.52*
z-axis Force	meas	3	1,028	4,746	*4,856*
	pred	7	888	4,676	*4,759*
	factor	2.58	0.86	0.99	*0.98*

Table 1: Broadband transfer function metric comparison between the predicted and measured transfer functions of the MPI Testbed.

diction accuracy to within a factor of three for this closed-loop case. Although, not as good as the open-loop case [7], the results are satisfactory given the additional complexities of the closed-loop model. Ongoing activities include improvement of the control model fidelity, validation of the methodology for passive and active vibration isolation, inclusion of disturbance torque transfer functions in the validation, and assessment of the sensitivity of these results to the accuracy and fidelity of the structural model.

References

[1] G. W. Neat, A. Abramovici, J. W. Melody, R. J. Calvet, N. M. Nerheim, and J. F. O'Brien, "Control technology readiness for spaceborne optical interferometer missions," in *Proc. Space Microdynamics and Accurate Control Symposium*, (Toulouse, France), May 1997.

[2] *TOPS: Towards Other Planetary Systems.* Washington, D.C.: National Aeronautics and Space Administration, Solar System Exploration Division, 1992.

[3] M. Shao and D. M. Wolf, "Orbiting stellar interferometer," in *Spaceborne Interferometry II* (R. D. Reasenberg, ed.), vol. 2447 of *Proc. SPIE*, (Orlando, FA), pp. 228–239, Apr. 1995.

[4] R. A. Laskin, "Technology for space optical interferometry," in *Proc. 33rd Aerospace Sciences Meeting and Exhibit*, vol. 95–0825, (Reno, NV), AIAA, Jan. 1995.

[5] M. H. Milman, H. C. Briggs, W. Ledeboer, J. W. Melody, R. L. Norton, and L. Needels, *Integrated Modeling of Optical Systems User's Manual, Release 2.0*, Nov. 1995. JPL D–13040.

[6] D. Redding, *Controlled Optics Modelling Package User Manual, Release 1.0*, June 1992. JPL D–9816.

[7] J. W. Melody and G. W. Neat, "Integrated modeling methodology validation using the micro-precision interferometer testbed," in *Proc. 35th IEEE Conference on Decision and Control*, vol. 4, (Kobe, Japan), pp. 4222–4227, Dec. 1996.

[8] J. R. Red-Horse, E. L. Marek, and M. B. Levine-West, "System identification of the jpl micro-precision interferometer truss: Test-analysis reconciliation," in *Proc. 34th SDM*, (La Jolla, CA), Apr. 1993.

[9] M. B. Levine-West and J. W. Melody, "Model updating of evolutionary structures," in *Proc. 15th ASME Biennial Conference on Mechanical Vibration and Noise*, (Boston, MA), Sept. 1995.

[10] S. Shaklan, J. Yu, and H. C. Briggs, "Integrated structural and optical modeling of the orbiting stellar interferometer," in *Space Astronomical Telescope and Instrument II, Proc. SPIE*, (Orlando, FA), Apr. 1993.

[11] B. J. Lurie, *Feedback Maximization*. Artech House, Inc., 1987.

[12] G. W. Neat and J. F. O'Brien, "Micro-precision interferometer testbed: Fringe tracker control system," in *Proc. 19th Annual AAS Guidance and Control Conference*, (Breckenridge, CO), Feb. 1996.

[13] J. T. Spanos, Z. Rahman, C.-C. Chu, and J. F. O'Brien, "Control structure interaction in long baseline space interferometers," in *Proc. 12th IFAC Symposium on Automatic Control in Aerospace*, (Ottobrunn, Germany), Sept. 1992.